

This document is the Accepted Manuscript version of a Published Work that appeared in final form in *ACS catalysis*, copyright © 2020 American Chemical Society after peer review and technical editing by the publisher. To access the final edited and published work see

<http://dx.doi.org/10.1021/acscatal.9b04451>.

This document is confidential and is proprietary to the American Chemical Society and its authors. Do not copy or disclose without written permission. If you have received this item in error, notify the sender and delete all copies.

**The Effects of Zr-doping into Ceria for the Dry Reforming of Methane over Ni/CeZrO<sub>2</sub> catalysts: In-situ Studies with XRD, XAFS and AP-XPS**

Journal:	<i>ACS Catalysis</i>
Manuscript ID	cs-2019-04451m.R2
Manuscript Type:	Article
Date Submitted by the Author:	03-Jan-2020
Complete List of Authors:	Zhang, Feng; Stony Brook University Liu, Zongyuan; Brookhaven National Laboratory, Chemistry Chen, Xiaobo; Binghamton University Rui, Ning; Brookhaven National Laboratory, Betancourt, Luis; Brookhaven National Laboratory, Chemistry Lin, Lili; Brookhaven National Laboratory, Chemistry Xu, Wenqian; X-ray Science Division Advanced Photon Source, Argonne National Laboratory Sun, Cheng-Jun; Argonne National Laboratory, Advanced Photon Source Abeykoon, A. M.; Brookhaven National Laboratory, Photon Sciences Rodriguez, Jose; Brookhaven National Laboratory, Chemistry Lorber, Kristijan; National Institute of Chemistry Slovenia, department of inorganic chemistry and technology Teržan, Janvit; Kemijski institut, D05 Djinovic, Petar; Kemijski institut, Department of Environmental Sciences and Engineering Senanayake, Sanjaya; Brookhaven National Laboratory, Chemistry

SCHOLARONE™  
Manuscripts

1  
2  
3 **The Effects of Zr-doping into Ceria for the Dry Reforming of Methane over**  
4 **Ni/CeZrO<sub>2</sub> Catalysts: *In-situ* Studies with XRD, XAFS and AP-XPS**  
5  
6  
7  
8  
9

10 Feng Zhang,<sup>1</sup> Zongyuan Liu,<sup>2</sup> Xiaobo Chen,<sup>3</sup> Ning Rui,<sup>2</sup> Luis E. Betancourt,<sup>2</sup> Lili, Lin,<sup>2</sup>  
11  
12 Wenqian Xu,<sup>4</sup> Chengjun Sun,<sup>4</sup> A. M. Milinda Abeykoon,<sup>5</sup> José A. Rodriguez,<sup>1,2</sup> Janvit Teržan,<sup>6</sup>  
13  
14 Kristijan Lorber,<sup>6</sup> Petar Djinović<sup>6\*</sup> and Sanjaya D. Senanayake<sup>2\*</sup>  
15  
16  
17  
18

19 <sup>1</sup> Materials Science and Chemical Engineering Department, Stony Brook University, Stony  
20 Brook, NY 11794, USA  
21

22 <sup>2</sup> Chemistry Division, Brookhaven National Laboratory, Upton, NY 11973, USA  
23

24 <sup>3</sup> Program of Materials Science and Engineering, Department of Mechanical  
25 Engineering, State University of New York at Binghamton,  
26 NY 13902, USA.  
27  
28

29 <sup>4</sup> X-ray Science Division, Advanced Photon Source, Argonne National Laboratory, Lemont, IL  
30 60439, USA  
31  
32

33 <sup>5</sup> Photon Science Division, National Synchrotron Light Source II, Upton, 11973 NY, USA  
34

35 <sup>6</sup> Department of Inorganic Chemistry and Technology, National Institute of Chemistry,  
36 Hajdrihova 19, SI-1001 Ljubljana, Slovenia  
37  
38

39  
40  
41 Corresponding Authors: Petar Djinović [petar.djinovic@ki.si], Sanjaya D. Senanayake

42  
43 [[ssenanay@bnl.gov](mailto:ssenanay@bnl.gov)]  
44  
45  
46  
47  
48  
49  
50  
51  
52  
53  
54  
55  
56  
57

**ABSTRACT**

The methane activation and methane dry reforming reactions were studied and compared over 4 wt% Ni/CeO<sub>2</sub> and 4 wt% Ni/CeZrO<sub>2</sub> (containing 20 wt% Zr) catalysts. Upon the incorporation of Zr into the ceria support, the catalyst exhibited a significantly improved activity and H<sub>2</sub> selectivity. To understand the effects of the Zr dopant on Ni and CeO<sub>2</sub> during the DRM reaction and to probe the structure–reactivity relationship underlying the enhanced catalytic performance of the mixed-oxide system, *in-situ* Time Resolved X-ray diffraction (TR-XRD), X-ray absorption fine structure (XAFS) and ambient-pressure X-ray photoelectron spectroscopy (AP-XPS) were employed to characterize the catalysts under the reaction conditions. The TR-XRD and AP-XPS indicate ceria-zirconia supported Ni (Ni/CeZrO<sub>2</sub>) is of higher reducibility than the pure ceria supported Ni/CeO<sub>2</sub> upon the reaction with pure CH<sub>4</sub> or for the methane dry reforming reaction. The active state of the Ni/CeZrO<sub>2</sub> under optimum DRM conditions (700 °C) was identified as Ni<sup>0</sup>, Ce<sup>3+</sup>/Ce<sup>4+</sup> and Zr<sup>4+</sup>. The particle size of both nickel and the ceria support under the reaction conditions were analyzed by Rietveld refinement and EXAFS fitting. The Zr in the ceria support prevents particle sintering and maintains small particle sizes for both metallic nickel and the partially reduced ceria support under reaction conditions, through a stronger metal-support interaction. Additionally, Zr prevents Ni migration from the surface into ceria forming a Ce<sub>1-x</sub>Ni<sub>x</sub>O<sub>2-y</sub> solid solution, which is seen in Ni/CeO<sub>2</sub>, thus helps to preserve the active Ni<sup>0</sup> on the Ni/CeZrO<sub>2</sub> surface.

**KEYWORDS:** nickel, ceria, zirconia, CeZrO<sub>2</sub> solid solution, XRD, XAFS, AP-XPS, dry reforming of methane

## 1. INTRODUCTION

The ability to simultaneously activate, then convert both CH<sub>4</sub> and CO<sub>2</sub> into useful intermediates or products through a catalytic process offers viable solutions for sustainable commercial fuel processing, and a practical solution to the irreversible and harmful impact of global greenhouse gas emissions.<sup>1-4</sup> Often, both CH<sub>4</sub> and CO<sub>2</sub> are found together in fossil fuels, bio fuels or land fill sources and there is a steep energy cost for the sequestration, separation and conversion of purified components prior to processing.<sup>5-6</sup> The catalytic Dry Reforming of Methane reaction (DRM: CH<sub>4</sub> + CO<sub>2</sub> ↔ 2CO + 2H<sub>2</sub>), is one way in which the direct production of synthesis gas (CO + H<sub>2</sub>) can be obtained from both chemically robust reactants without the need of additional steps in conversion.

Our recent work has highlighted the metal-oxide interface and interactions in supported and inverse catalysts as key factors for achieving new pathways for activating CH<sub>4</sub> and CO<sub>2</sub> simultaneously at low temperatures.<sup>7-10</sup> Our primary focus has been on the M-CeO<sub>2</sub> class of catalysts, including M = Co, Ni, Fe, Cu, Ru in intimate contact with the surfaces of ceria supports. Our observations have shown that the chemical role of the metal can be distinct, while a special relationship between the metal and support at low coverages, with high dispersion occurs with the reduced Ce<sup>3+</sup> rich surfaces that can achieve catalytic chemistry not possible with bulk metals or pure oxide surfaces. This concept is supported by previous studies demonstrating the important role of the ceria support to anchor and then activate metals with high chemical potential.<sup>11</sup>

In this work we have extended the study to the modification of the ceria support, to explore if similar chemistry is observed for the M-Ceria interaction, in the presence of a commonly used dopant such as Zr. It has been extensively reported that by introducing dopants such as Zr, La or W into ceria, the oxygen storage capacity and reducibility of the ceria support could be enhanced.<sup>12-15</sup> Previous studies also found increased catalytic activity for CO and CO<sub>2</sub> methanation, selective oxidation of ethanol and also DRM reaction when metal was supported on a CeO<sub>2</sub>-ZrO<sub>2</sub> mixed oxide rather than on pure ceria.<sup>16-21</sup> However, the origin behind the improved DRM reaction activity and the chemical/structural behaviors of both metal, Zr dopant and ceria support under challenging DRM reaction conditions has not been completely elucidated.

1  
2  
3 The ability to enhance the propensity for dry reforming chemistry is limited by our fundamental  
4 knowledge of the nature of catalyst surfaces and direct evidence for transformations that occur  
5 under difficult reaction conditions. Such an understanding requires observations of the process as  
6 they are taking place or *in-situ* using multiple probes of the catalyst, including the chemical,  
7 electronic and structural active state of the material ideally in similar reaction conditions. An  
8 added complication for the DRM process is the need for high temperatures (> 400 °C) for  
9 sustained turnover, necessitating characterization at challenging temperature limits, often  
10 unachievable in many *in-situ* analytical techniques. In this study we utilize several commonly  
11 used techniques including XRD, XAFS and XPS but under elevated temperature and *in-situ* DRM  
12 conditions. We aim to unravel the reasons for improved DRM reaction performance with Zr  
13 dopants and establish a detailed autopsy of chemical and structural properties and role of Ni and  
14 Ce with and without Zr dopants as the DRM reaction proceeds.  
15  
16  
17  
18  
19  
20  
21  
22  
23

## 24 2. EXPERIMENTAL

25  
26 **2.1. Catalyst synthesis.** During the synthesis of the CeZrO<sub>2</sub> mixed oxide (containing around  
27 20 wt% of Zr, and Ce:Zr atomic ratio is 3:1), 1.09 g of ZrO(NO<sub>3</sub>)<sub>2</sub>\*6H<sub>2</sub>O was dissolved in 5 ml  
28 of ultrapure water during sonication. After dissolution, 4.04 g of Ce(NO<sub>3</sub>)<sub>3</sub>\*6H<sub>2</sub>O was added and  
29 mixed until complete dissolution. Afterwards, 5 ml of propionic acid and 154 ml of ethylene  
30 glycol were added, and the solution was mixed for an additional 15 min, transferred to Teflon<sup>®</sup>  
31 clad stainless-steel autoclaves and treated at 180 °C for 200 min. The autoclaves were quench  
32 cooled, the slurry centrifuged and calcined in air for 4 h at 450°C. Synthesis of pure CeO<sub>2</sub> and  
33 ZrO<sub>2</sub> followed the same protocol as above, whereas only their individual precursor was used.  
34  
35  
36  
37  
38  
39

40 The 4 wt% nickel was deposited by slow addition of NH<sub>4</sub>OH to the aqueous CeO<sub>2</sub> or CeZrO<sub>2</sub>  
41 suspension containing an appropriate amount of dissolved Ni(NO<sub>3</sub>)<sub>2</sub>. The pH of the suspension  
42 was raised to 9.5 over the course of 2 h, and the suspension was centrifuged, dried overnight at  
43 70 °C and calcined in air for 4 h at 450 °C.  
44  
45  
46

47 **2.2. Catalytic performance tests.** The DRM catalytic performance of 4 wt% Ni/CeO<sub>2</sub> and 4  
48 wt% Ni/CeZrO<sub>2</sub> catalysts were compared through the conversion, reaction rate and selectivity. A  
49 10 mg powder catalyst diluted with a ~ 30 mg pre-calcined quartz (900 °C) were loaded into a  
50 quartz tube and mounted on a plug flow reactor system. The catalysts were pre-reduced in 25  
51 cc/min H<sub>2</sub> and 25 cc/min He mixture at 450 °C for 30 min before switching to the DRM reaction  
52 gas mixture (10 cc/min CH<sub>4</sub>, 10 cc/min CO<sub>2</sub> and 30 cc/min N<sub>2</sub>) at room temperature (weight  
53  
54  
55  
56  
57  
58  
59  
60

hourly space velocity: 300,000 ml/g<sub>cat</sub>/h). The catalysts were then heated stepwise from room temperature to 700 °C with isothermal steps at 200, 300, 400, 500, 600, and 700 °C for 1 hour. The residual gas products were analyzed by a gas chromatography instrument (Agilent 7890A) equipped with flame ionization and thermal conductivity detectors, and the conversions, reaction rates were calculated employing the equations S1-S5. The H<sub>2</sub> selectivity was defined as the amount of H<sub>2</sub> produced with respect to the total H<sub>2</sub> and H<sub>2</sub>O production (Equation S6).

### 2.3. Characterizations

**2.3.1. Pair Distribution Function (PDF) and XRD.** The PDF spectra of Ni/CeO<sub>2</sub> and Ni/CeZrO<sub>2</sub> samples, along with calcined CeO<sub>2</sub>, ZrO<sub>2</sub> and NiO standards were collected at 28ID ( $\lambda = 0.1667 \text{ \AA}$ ) of National Synchrotron Light Source (NSLS-II) of Brookhaven national Laboratory (BNL). The sample was loaded into a 1 mm OD, and 0.9 mm ID Kapton tube for the measurement, and PDFget3 was used to process the results.<sup>22</sup> The *ex-situ* and *in-situ* time-resolved XRD analyses were carried out at 17BM ( $\lambda = 0.24108 \text{ \AA}$ ) of the Advanced Photon Source (APS), at Argonne National Laboratory (ANL). A Clausen cell flow reactor was used for the *in-situ* methane activation and methane dry reforming measurement.<sup>23</sup> For the methane activation study, a gas mixture of 5 cc/min CH<sub>4</sub> and 5 cc/min He was introduced to around 2 mg of catalyst in the flow cell, and the sample was heated from room temperature to 700 °C with a 5 °C/min ramping rate under the methane atmosphere. For the dry reforming reaction, the sample (~2 mg) was pre-reduced under 5 cc/min H<sub>2</sub> and 5 cc/min He at 450 °C for 30 min, and a 2 cc/min CH<sub>4</sub>, 2 cc/min CO<sub>2</sub> and 6 cc/min He gas mixture was used afterwards for the DRM reaction. The catalysts were heated stepwise from room temperature to 700 °C with a 10 °C/min ramping rate and 1-hour soak time at 200, 300, 400, 500, 600, and 700 °C temperature stages. An amorphous Si flat panel (Perkin Elmer) detector was used to collect two-dimensional XRD images throughout the reaction processes, and the images were subsequently processed with GSAS-II to obtain diagrams of Intensity versus  $2\theta$ . Rietveld analyses were also performed through GSAS-II to obtain information such as lattice parameter and crystallite size.<sup>24</sup>

**2.3.2. Transmission electron microscopy (TEM) and energy-dispersive X-ray spectroscopy (EDS).** TEM, HAADF-STEM (high-angle annular dark field scanning transmission electron microscopy) and EDS element mapping were performed using a high-resolution analytical scanning/transmission electron microscope (S/TEM, FEI Talos F200X) operating at 200 keV at

1  
2  
3 the Center for Functional Nanomaterials (CFN) of Brookhaven National Laboratory (BNL). The  
4 post-reaction catalysts were collected immediately after it was cooled down from the DRM  
5 reaction condition at 700 °C to room temperature, and then dispersed in methanol by sonication.  
6 A droplet of suspension was introduced onto Holey-Carbon coated Cu grids and allowed to dry  
7 before imaging. The elemental mappings (Ni K-edge, Ce L-edge, Zr L-edge) were acquired with  
8 a four-quadrant 0.9-sr energy dispersive X-ray spectrometer (Super EDS).  
9

10  
11  
12 **2.3.3. XAFS.** In-situ X-ray absorption near edge structure and (XANES) and extend X-ray  
13 absorption fine structure (EXAFS) during the DRM reaction on Ni/CeO<sub>2</sub> and Ni/CeZrO<sub>2</sub> were  
14 collected at the 20ID beamline of the Advanced Photon Source (APS), at Argonne National  
15 Laboratory (ANL). Approximately 2 mg samples were loaded into a Clausen cell and mounted in  
16 line with a gas flow system. The reaction conditions including the gas flow rate and the  
17 temperature profile were kept the same as the in-situ XRD measurements (2.3.1) for pre-treatment  
18 and for the DRM reaction. The Ni K-edge data was collected using fluorescence yield by a four-  
19 channel Vortex detector. At each temperature stage, three parallel spectra were collected and  
20 averaged together to improve the quality of the data. Data processing was performed using the  
21 IFEFFIT package and Nickel foil was used as the standard reference for the EXAFS fitting.<sup>25</sup>  
22

23  
24 **2.3.4. AP-XPS.** A commercial SPECS AP-XPS chamber equipped with a PHOIBOS 150 EP  
25 MCD-9 analyzer at the Chemistry Division of Brookhaven National Laboratory (BNL) was used  
26 for AP-XPS analysis (Mg K $\alpha$  anode; 30 eV pass energy; 0.1eV step size and energy resolution  
27 ~0.4 eV).<sup>26</sup> The powder catalyst was pressed onto an aluminum plate and loaded into the AP-XPS  
28 chamber. During the CH<sub>4</sub> activation process, 30 mTorr of CH<sub>4</sub> was introduced into the analysis  
29 chamber, and Ni 1s, Ce 3d and Zr 3d spectra were collected at 25, 200, 300, 400, and 500 °C. For  
30 the DRM reaction measurements, 20 mTorr of H<sub>2</sub> were used to pretreat the samples at 450 °C for  
31 30 min in the analysis chamber. After evacuation of the H<sub>2</sub>, a gas mixture of 30 mTorr CH<sub>4</sub> and  
32 30 mTorr CO<sub>2</sub> was introduced into the analysis chamber, and the Ni 1s, Ce 3d and Zr 3d spectra  
33 were collected at 25, 200, 300, 400 and 500 °C under reaction conditions. The Ce 3d  
34 photoemission line with the strongest Ce<sup>4+</sup> feature (916.9 eV) was used for the energy calibration  
35 of Ni 1s and Ce 3d peaks and C 1s (at 284.6 eV) was used for the energy calibration of Zr 3d  
36 spectra.  
37  
38  
39  
40  
41  
42  
43  
44  
45  
46  
47  
48  
49  
50  
51  
52

### 53 54 55 **3. RESULTS AND DISCUSSION**

### 3.1. Structural and morphological properties of the Ni/CeZrO<sub>2</sub> and Ni/CeO<sub>2</sub> catalysts.

Figure 1a shows the XRD patterns of the Ni/CeZrO<sub>2</sub> and Ni/CeO<sub>2</sub> samples as well as ZrO<sub>2</sub> and CeO<sub>2</sub> references. The green dashed line in the figure designates the position of the CeO<sub>2</sub> (111) diffraction peak and it demonstrates a broader CeO<sub>2</sub> (111) peak, shifted to a higher 2 theta value in the Ni/CeZrO<sub>2</sub> sample. The shift of the ceria peaks comes from the substitution of the smaller Zr<sup>4+</sup> (0.8 Å) ions into Ce<sup>4+</sup> sites (1.0 Å), and the consequent lattice contraction (~ 0.07Å) induced by Zr dopants. The absence of ZrO<sub>2</sub> diffraction peaks, the broadness and shift of CeO<sub>2</sub> peaks, evident in the XRD pattern of Ni/CeZrO<sub>2</sub> suggests the formation of a CeZrO<sub>2</sub> solid solution which adopts a simple ceria cubic fluorite structure<sup>27-30</sup>. The blue arrows (see also the insets in Figure 1a for the enlarged area) in the figure denote the presence of crystalline NiO in both Ni/CeZrO<sub>2</sub> and Ni/CeO<sub>2</sub> samples. The first and second shell PDF spectra of Ni/CeO<sub>2</sub> and Ni/CeZrO<sub>2</sub> samples with ZrO<sub>2</sub>, CeO<sub>2</sub> standards are provided in Figure 1b (See Figure S1 for the PDF spectra in long-range order). The mean bond lengths of the Ce-O pairs in the first shell of Ni/CeO<sub>2</sub> sample was the same as that in the CeO<sub>2</sub> standard, while in the Ni/CeZrO<sub>2</sub> sample, besides the Ce-O pairs at 2.35 Å, a shoulder at 2.13 Å was observed, which reflects the existence of Zr-O bonds. As for the second neighbor, the Ce-Ce pairs in Ni/CeO<sub>2</sub> sample and CeO<sub>2</sub> standard at 3.83 Å shifted to 3.79 Å in the Ni/CeZrO<sub>2</sub> sample, and there is no Zr-Zr feature shown in the Ni/CeZrO<sub>2</sub> sample. The peak shift is also consistent with the previous study by Milen Gateshki et al.,<sup>31</sup> which confirms the formation of a homogeneous CeZrO<sub>2</sub> solid solution in our Ni/CeZrO<sub>2</sub> sample.

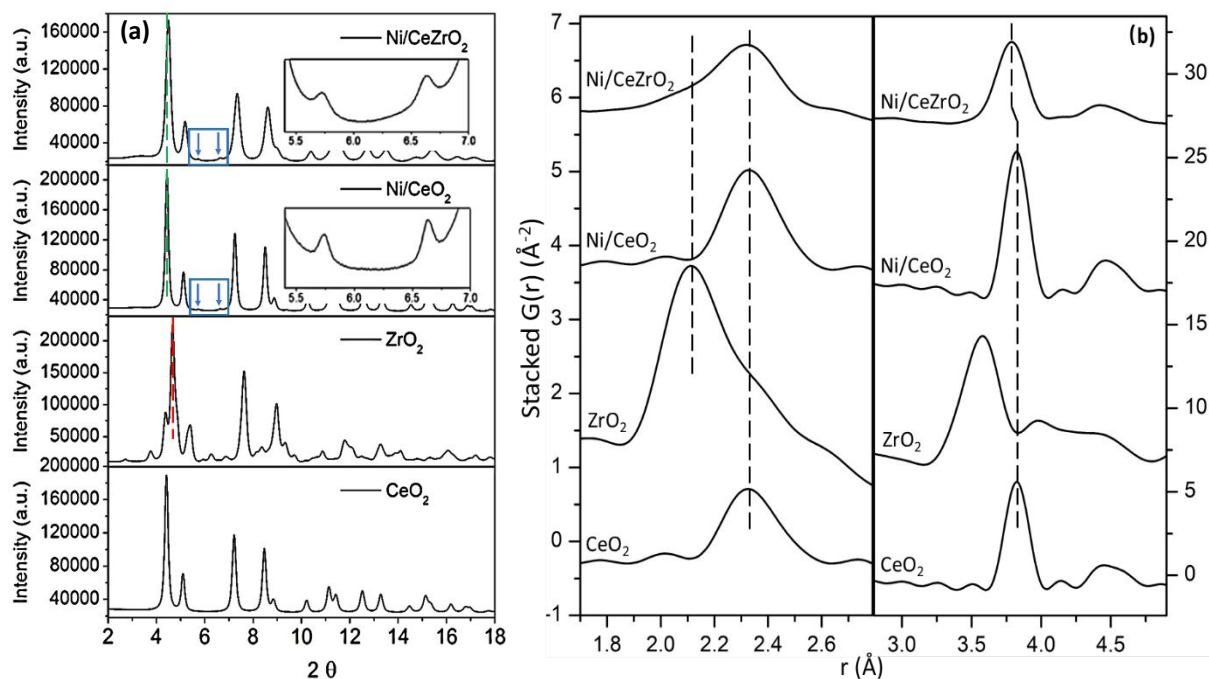


Figure 1. (a) XRD patterns of the synthesized Ni/CeZrO<sub>2</sub> and Ni/CeO<sub>2</sub> samples with ZrO<sub>2</sub> and CeO<sub>2</sub> XRD profiles as references. (b) PDF spectra of Ni/CeZrO<sub>2</sub> and Ni/CeO<sub>2</sub> samples with ZrO<sub>2</sub>, CeO<sub>2</sub> PDF profiles as references.

TEM and EDS mapping were conducted for all samples. Figure 2 shows the corresponding images for the post-reaction Ni/CeZrO<sub>2</sub> (Figure 2a) and Ni/CeO<sub>2</sub> (Figure 2b) catalysts in order to investigate the morphology and distributions of Ni/Zr and the influence of the DRM reaction (under stream for 1h at 700 °C). From Figure 2, it is obvious that both Ni and CeO<sub>2</sub> particles in the Ni/CeO<sub>2</sub> sample are larger than those in Ni/CeZrO<sub>2</sub>. The particle size for Ni is around 10 and 4 nm in Ni/CeO<sub>2</sub> and Ni/CeZrO<sub>2</sub>, respectively, while ceria is around 60 and 30 nm in Ni/CeO<sub>2</sub> and Ni/CeZrO<sub>2</sub>, respectively. Meanwhile, Zr preserves its homogeneous distribution, indicating CeZrO<sub>2</sub> mixed oxide maintains its stable structure under the DRM reaction even at 700 °C. Carbon deposition was observed in post reaction Ni/CeO<sub>2</sub> samples (Figure S2) in the form of filamentous fibers and larger carbon composites. Relatively, the Ni/CeZrO<sub>2</sub> sample showed less evidence of total carbon presence.

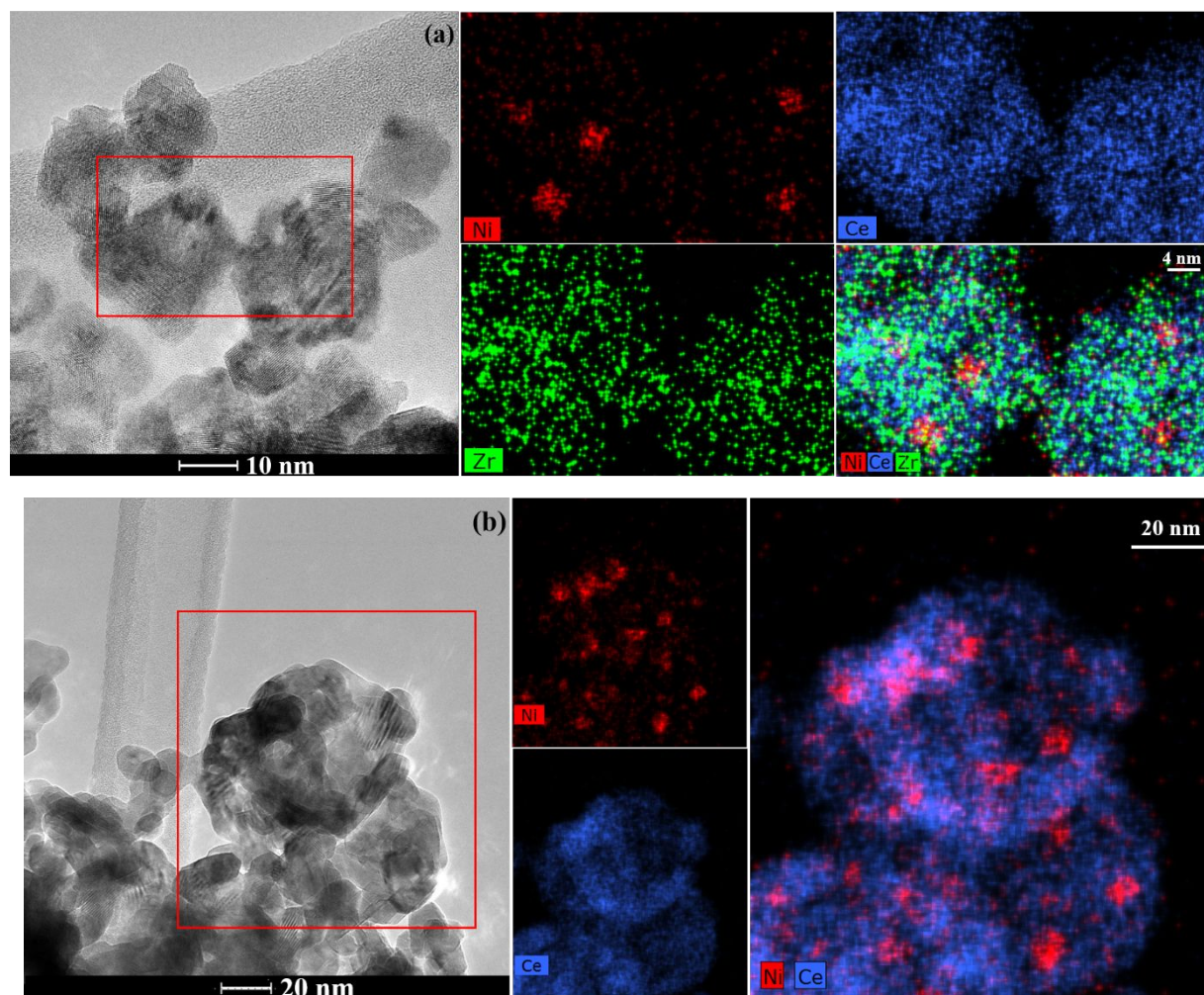


Figure 2. TEM and EDS mapping of Ni/CeZrO<sub>2</sub> catalyst (a) and Ni/CeO<sub>2</sub> catalyst (b) after the DRM reaction at 700 °C.

**3.2. Catalytic performance of Ni/CeZrO<sub>2</sub> and Ni/CeO<sub>2</sub> for the DRM reaction .** The catalytic performance of both samples was compared through conversion, reaction rate and H<sub>2</sub> selectivity, and the results are presented in Figure 3. Higher DRM reaction activity was observed with Ni/CeZrO<sub>2</sub> than with Ni/CeO<sub>2</sub> through all temperature ranges. At 500 °C, the conversion of CH<sub>4</sub> and CO<sub>2</sub> on Ni/CeZrO<sub>2</sub> was 8% and 15%, respectively, which is close to the thermodynamic equilibrium.<sup>32</sup> When the temperature reaches 700 °C, the conversion of CH<sub>4</sub> increased to around 51% and the conversion of CO<sub>2</sub> was 66%; this is ~1.5 times the conversion than that was observed on the Ni/CeO<sub>2</sub> catalyst. Only H<sub>2</sub>O, H<sub>2</sub>, and CO were detected via GC and RGA (RGA spectra are provided in Figure S3) as the products, and the reaction rate of H<sub>2</sub>O, H<sub>2</sub> and CO were 67, 710 and 960 μmol/g<sub>cat</sub>/s, respectively. The reverse water gas shift reaction (RWGS: H<sub>2</sub> + CO<sub>2</sub> ↔ H<sub>2</sub>O

+ CO) is one of the undesirable side reactions accompanying DRM, which consumes a product ( $H_2$ ) and transforms it to  $H_2O$ , thus reducing  $H_2$  selectivity and the  $H_2/CO$  stoichiometric ratio.<sup>33-34</sup> From Figure 3c, we can see that  $H_2$  selectivity rises with increasing temperature, and, at different temperatures, it remains higher on  $Ni/CeZrO_2$  than on  $Ni/CeO_2$ . This suggests a suppression of the RWGS reaction at higher temperatures with the assistance of Zr in the support.<sup>35-37</sup> Overall,  $Ni/CeZrO_2$  exhibits better catalytic performance than  $Ni/CeO_2$ , with a higher  $CH_4$  and  $CO_2$  conversion, higher reaction rate, and a higher selectivity for  $H_2$ .

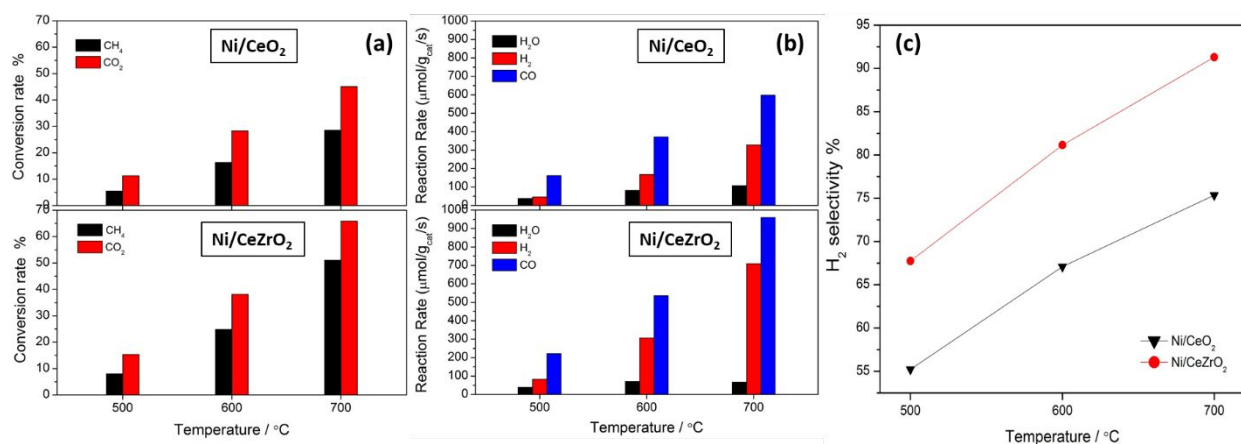


Figure 3. Comparison of the conversion (a), Reaction rate (b), and  $H_2$  selectivity (c) for the DRM reaction over  $Ni/CeO_2$  and  $Ni/CeZrO_2$  samples. Reaction conditions: 10 cc/min  $CO_2$  + 10 cc/min  $CH_4$  + 30 cc/min  $N_2$  with 10 mg of the catalyst; weight hourly space velocity (WHSV): 300,000  $ml/(g_{cat} \cdot h)$ .

**3.3. Methane activation of the  $Ni/CeZrO_2$  and  $Ni/CeO_2$  catalysts.** Figure 4 shows the sequential XRD profiles of the  $Ni/CeZrO_2$  and  $Ni/CeO_2$  samples under a reductive  $CH_4$  atmosphere with a ramping temperature from 25 to 700 °C. The identified NiO (peaks at 5.7° and 6.6°) in the as-prepared samples was reduced at around 400 °C in both  $Ni/CeZrO_2$  and  $Ni/CeO_2$ . As for the  $CeO_2$  support, a significant increase in the intensity of the ceria diffraction peaks for the  $Ni/CeO_2$  sample was observed at high temperatures, while peaks for the  $Ni/CeZrO_2$  sample remained relatively stable. This indicates more pronounced  $CeO_2$  particle sintering in  $Ni/CeO_2$  than in  $Ni/CeZrO_2$ . The evolution of the ceria lattice parameter was obtained from Rietveld refinement (Figure 5). The smaller oxide lattice parameter in  $Ni/CeZrO_2$  sample at room temperature (5.35 vs 5.42 Å for pure ceria) comes from a lattice contraction induced by replacing

1  
2  
3  $\text{Ce}^{4+}$  with smaller  $\text{Zr}^{4+}$  in the ceria lattice<sup>27-29</sup>. However, as the temperature increased towards 400  
4 °C, a more substantial ceria lattice expansion was observed in  $\text{Ni/CeZrO}_2$  than in  $\text{Ni/CeO}_2$ . In  
5 addition to the linear lattice expansion caused by thermal effects, the abrupt increase of the oxide  
6 lattice parameter indicates the reduction of  $\text{Ce}^{4+}$  (1.28 Å ionic radius) to  $\text{Ce}^{3+}$  (1.48 Å ionic radius)  
7 and the repulsion between the oxygen vacancies and their surrounding cations.<sup>38-40</sup> Even though  
8 the thermal expansion coefficient (TEC) of zirconia doped ceria was reported to be slightly larger  
9 than pure ceria,<sup>41</sup> the conspicuously sharper increase of the ceria lattice in  $\text{Ni/CeZrO}_2$  sample  
10 around 400 °C suggests a greater reducibility of the ceria support by methane due to the presence  
11 of Zr dopants.  
12

13  
14  
15  
16  
17  
18  
19 Indeed, temperature programmed reduction of  $\text{Ni/CeO}_2$  and  $\text{Ni/CeZrO}_2$  with  $\text{H}_2$  showed that  
20 35% more  $\text{H}_2$  was consumed during the reduction of the  $\text{Ni/CeZrO}_2$  sample between room  
21 temperature and 423 °C (Figure S4), confirming the higher reducibility of  $\text{CeZrO}_2$  solid solution  
22 support. Notably, an apparent increase of the ceria lattice parameter in the  $\text{Ni/CeO}_2$  sample was  
23 also detected between 600 and 700 °C under  $\text{CH}_4$  atmosphere, and this resulted in a ~ 0.14 Å total  
24 expansion (from room temperature to 700 °C) of ceria in  $\text{Ni/CeO}_2$ , which is comparable to the  
25 total lattice expansion of ceria in the  $\text{CeZrO}_2$  solid solution (~0.15 Å). This distinct expansion of  
26 ceria could be attributed to the bulk reduction of  $\text{Ce}^{4+}$  to  $\text{Ce}^{3+}$  in  $\text{Ni/CeO}_2$  only when the  
27 temperature reaches above 600 °C.<sup>42-43</sup>  
28  
29  
30  
31  
32  
33  
34  
35  
36  
37  
38  
39  
40  
41  
42  
43  
44  
45  
46  
47  
48  
49  
50  
51  
52  
53  
54  
55  
56  
57  
58  
59  
60

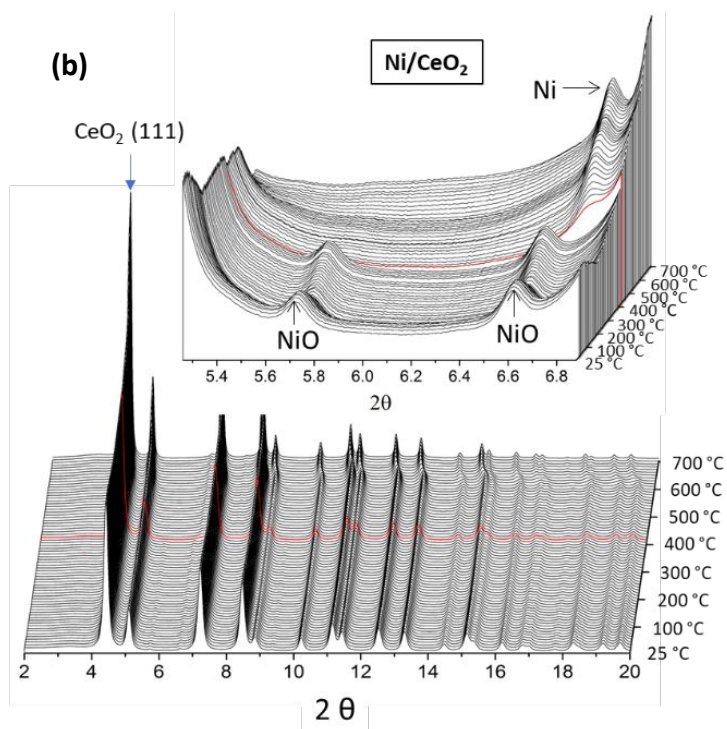
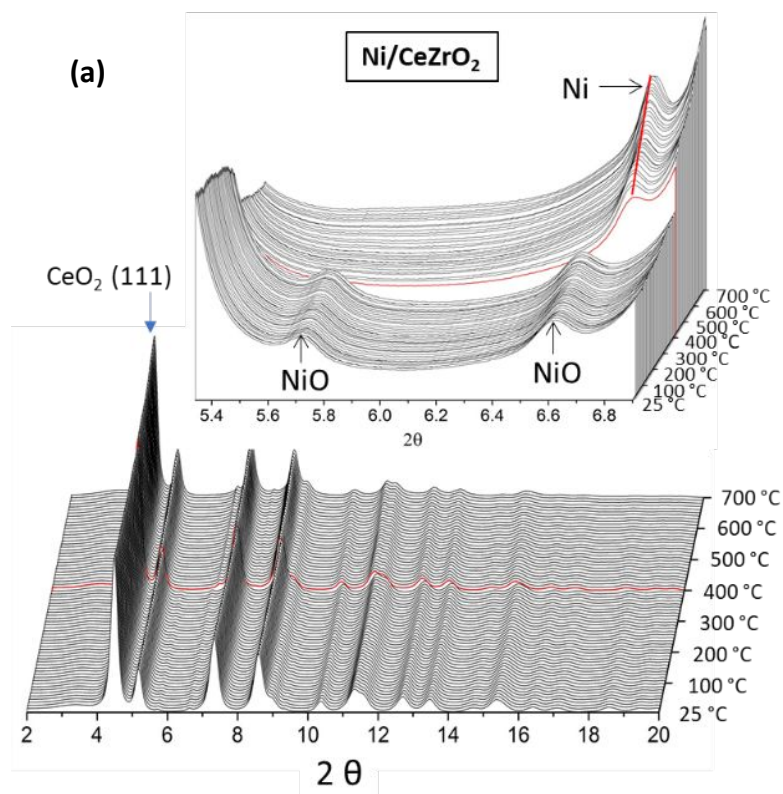


Figure 4. *In-situ* XRD profiles of Ni/CeZrO<sub>2</sub> (a) and Ni/CeO<sub>2</sub> (b) samples in a CH<sub>4</sub> atmosphere. Reaction conditions: 5 cc/min CH<sub>4</sub> + 5 cc/min He, ramping to 700 °C with a 5 °C ramping rate.

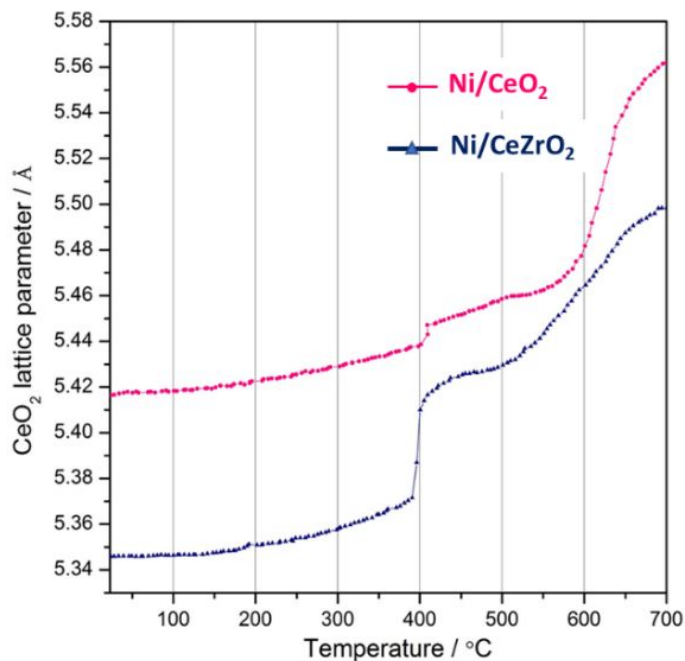


Figure 5. Ceria lattice parameter evolution as a function of temperature during the methane activation process. The results were generated from Rietveld refinement of *in-situ* XRD data using the GSAS-II software.

AP-XPS was conducted to follow the chemical state of the catalysts under methane activation conditions. Ce 3d and Ni 2p AP-XPS spectra for methane activation on Ni/CeZrO<sub>2</sub> and Ni/CeO<sub>2</sub> samples are presented in Figure 6. It is possible to observe a more intense Ce<sup>3+</sup> peak in Ni/CeZrO<sub>2</sub> than in Ni/CeO<sub>2</sub> at 400 and 500 °C, which validates the *in-situ* XRD results (Figure 5) that ceria is reduced to a larger extent in the Zr-doped support. The reduction of Ni<sup>2+</sup> to metallic Ni occurs at 400 °C, evident from the AP-XPS spectra for both Ni/CeZrO<sub>2</sub> and Ni/CeO<sub>2</sub> samples, which is also supported by the *in-situ* XRD results (Figure 4). The Ni 2p spectra were also fitted for both samples and the results are provided in Figure S5 and Table S1. The Ni 2p peaks of Ni/CeZrO<sub>2</sub> are noticeably larger and narrower than those of Ni/CeO<sub>2</sub>. With the same loading of Ni in both samples, the larger and narrower Ni 2p peak in Ni/CeZrO<sub>2</sub> suggests that more Ni<sup>0</sup> sites with smaller Ni<sup>0</sup> particles were exposed on this sample's surface when compared to the Ni/CeO<sub>2</sub>. In the Ni/CeZrO<sub>2</sub>, a higher dispersion of smaller Ni particles is due to a more defect rich and reactive

oxide support. The Zr 3d spectra were also collected and presented in Figure S6a, showing a stable  $Zr^{4+}$  chemical state throughout the entire reaction with methane.

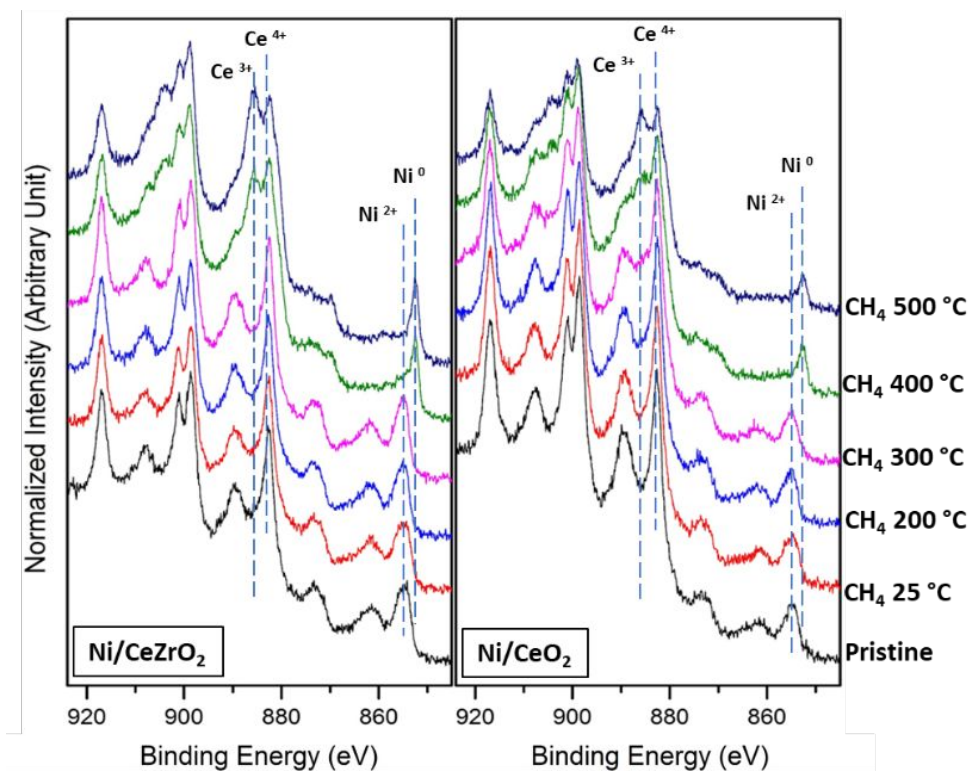
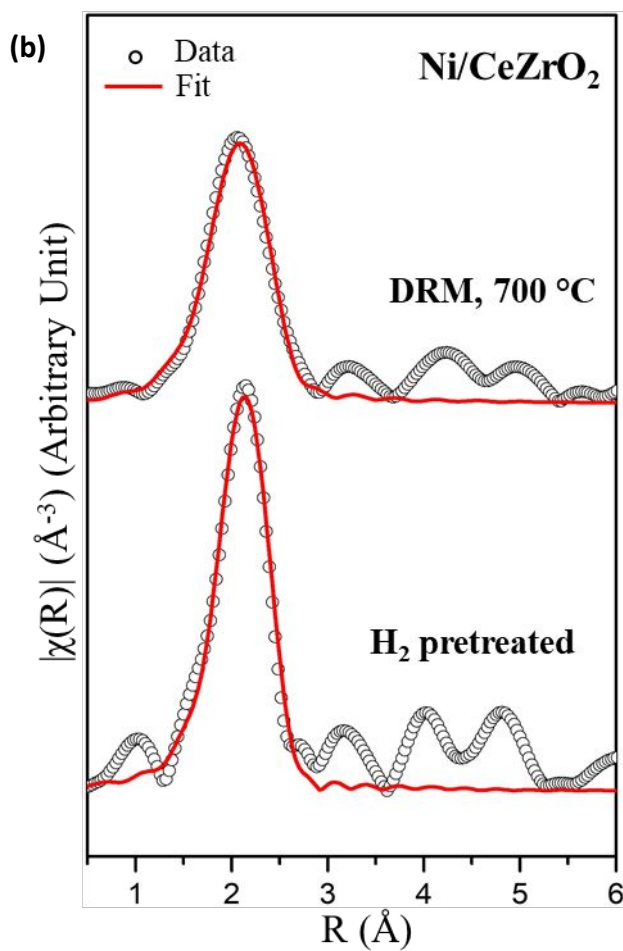
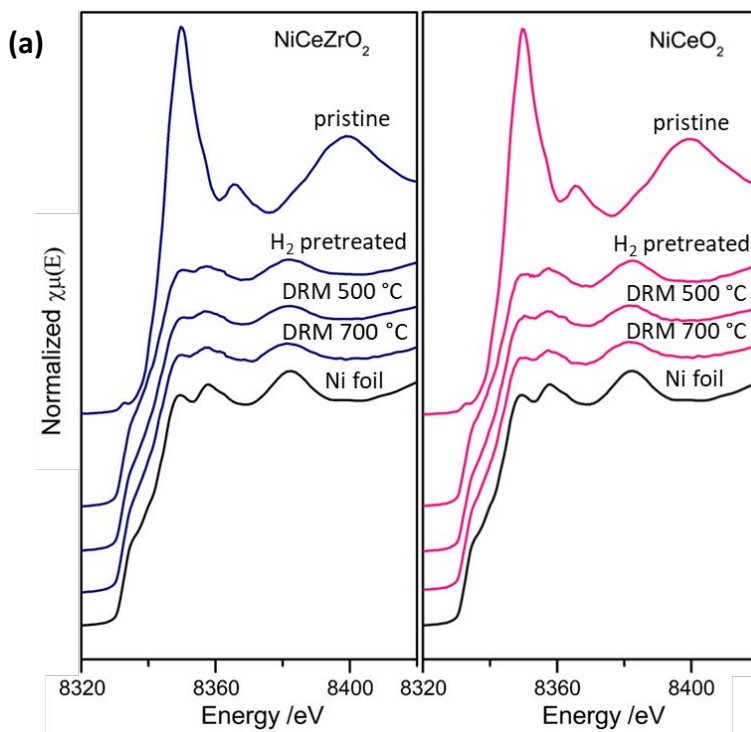
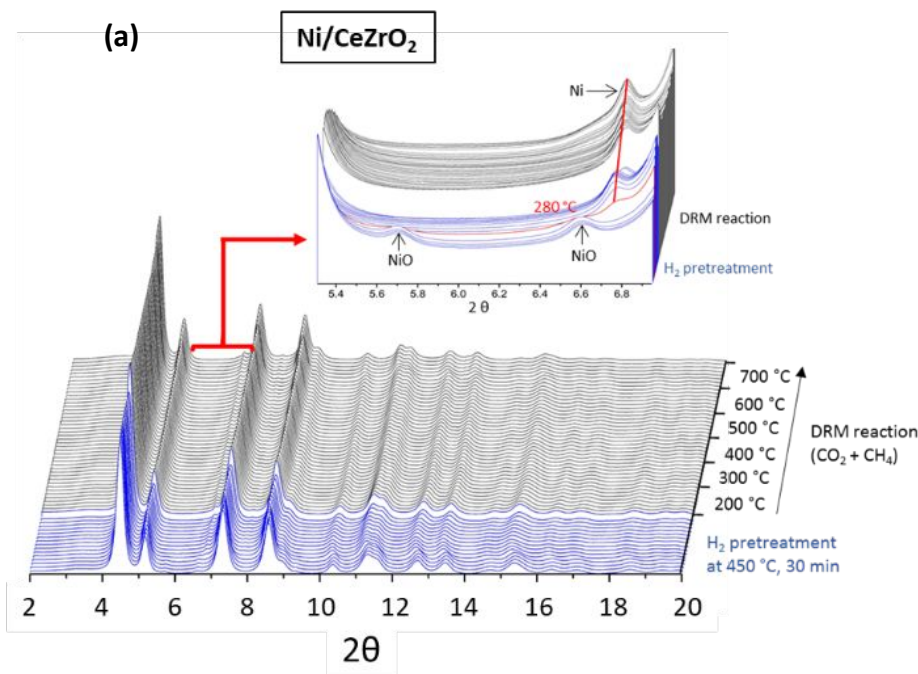


Figure 6. Ce 3d and Ni 2p AP-XPS spectra of Ni/CeZrO<sub>2</sub> and Ni/CeO<sub>2</sub> samples in a CH<sub>4</sub> atmosphere at elevated temperatures. Reaction conditions: 30 mTorr of CH<sub>4</sub> at temperatures of 25, 200, 300, 400, and 500 °C.

**3.4. Dry Reforming of Methane on the Ni/CeZrO<sub>2</sub> and Ni/CeO<sub>2</sub> catalysts.** We employed *in-situ* XANES and XRD measurements to elucidate the chemical and structural changes that occurred during the DRM reaction on the Ni/CeZrO<sub>2</sub> and Ni/CeO<sub>2</sub> catalysts. These results are shown in Figures 7a and 8, respectively. NiO was identified in the as-prepared Ni/CeZrO<sub>2</sub> and Ni/CeO<sub>2</sub> samples with both techniques, and it was reduced to metallic Ni during the H<sub>2</sub> pretreatment process (Figure 7a and Figure 8). The reduction temperatures of NiO during H<sub>2</sub> pretreatment were close for both samples (Figure 8), with Ni/CeZrO<sub>2</sub> (~280 °C) slightly higher than Ni/CeO<sub>2</sub> (~260 °C). The reduced Ni<sup>0</sup> maintains its metallic nature under the DRM reaction (CO<sub>2</sub> + CH<sub>4</sub> + He) from 500 to 700 °C, according to both XANES and XRD profiles in Figure 7a and 8, respectively.



1  
2  
3 Figure 7. (a) *In-situ* Ni K-edge XANES spectra of Ni/CeO<sub>2</sub> and Ni/CeZrO<sub>2</sub> samples with Ni foil  
4 spectra provided as the reference. (b) The Fourier-transformed R-space EXAFS spectra of  
5 Ni/CeZrO<sub>2</sub> sample after H<sub>2</sub> pretreatment and during the DRM reaction at 700 °C. (The catalyst  
6 (~ 2 mg) was pretreated in H<sub>2</sub> at 450 °C for 30 min before switching the gas to a mixture of 2  
7 cc/min CO<sub>2</sub> + 2 cc/min CH<sub>4</sub> + 6 cc/min He at room temperature. The sample was then heated  
8 under DRM reaction atmosphere from 25 to 700 °C with a 10 °C/min ramping rate. XAFS spectra  
9 were collected before and after H<sub>2</sub> pretreatment at 25 °C, and under the DRM reaction condition  
10 at 25, 500 and 700 °C.  
11  
12  
13  
14  
15  
16  
17



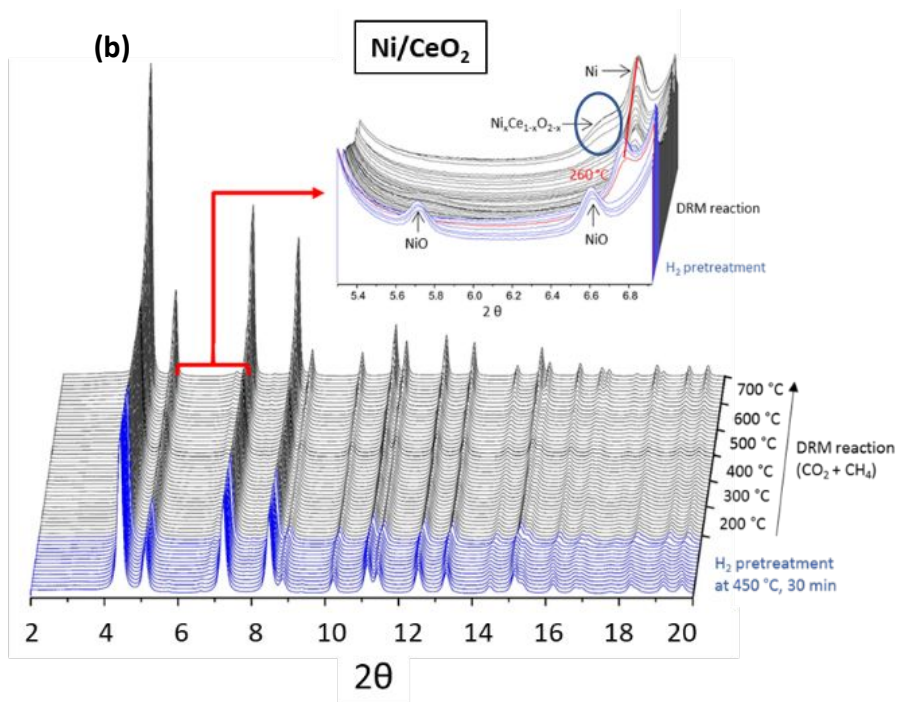


Figure 8. *In-situ* XRD profiles of Ni/CeZrO<sub>2</sub> (a) and Ni/CeO<sub>2</sub> (b) samples under DRM reaction conditions. The catalyst was pretreated in H<sub>2</sub> at 450 °C for 30 min before switching the gas to a mixture of 2 cc/min CO<sub>2</sub> + 2 cc/min CH<sub>4</sub> + 6 cc/min He at room temperature. The sample was then heated under DRM reaction atmosphere from 25 to 700 °C with a 10 °C/min ramping rate and 30 min soak time at each temperature stage of 200, 300, 400, 500, 600, and 700 °C).

The CeO<sub>2</sub> particle sintering was also observed for the Ni/CeO<sub>2</sub> sample during the methane dry reforming reaction (Figure 8b and 9a) as seen in pure methane (Figure 4b). The Rietveld refinement results in Figure 9a illustrate that the crystallite size of ceria in the Ni/CeO<sub>2</sub> sample increased from 16 to 60 nm at 700 °C while the corresponding increase of the ceria crystallite size in Ni/CeZrO<sub>2</sub> was only ~ 14 nm (increasing from 19 to 33 nm). The crystallite sizes of ceria support calculated by the Rietveld refinement are also consistent with the EDS mapping results shown in Figure 2, indicating that the ceria particles in both samples are all crystalline. Figure 9b demonstrates that the lattice parameter of ceria in Ni/CeZrO<sub>2</sub> is always smaller than that in the Ni/CeO<sub>2</sub> sample during the reaction below 700 °C. This can be attributed to the introduction of smaller Zr<sup>4+</sup> ions into ceria support which also creates a contraction strain and decrease of the total ceria lattice parameter.<sup>27-29</sup> However, when the temperature increased to 700 °C during DRM, the initially smaller ceria lattice in the Ni/CeZrO<sub>2</sub> sample expanded significantly to a value even

larger than the ceria lattice parameter of the Ni/CeO<sub>2</sub>. This expansion signifies the severe reduction of the ceria support in the Ni/CeZrO<sub>2</sub> sample when the temperature reached 700 °C under the DRM reaction condition,<sup>38-39, 42-43</sup> indicating the improved reducibility of the ceria support with Zr dopants.

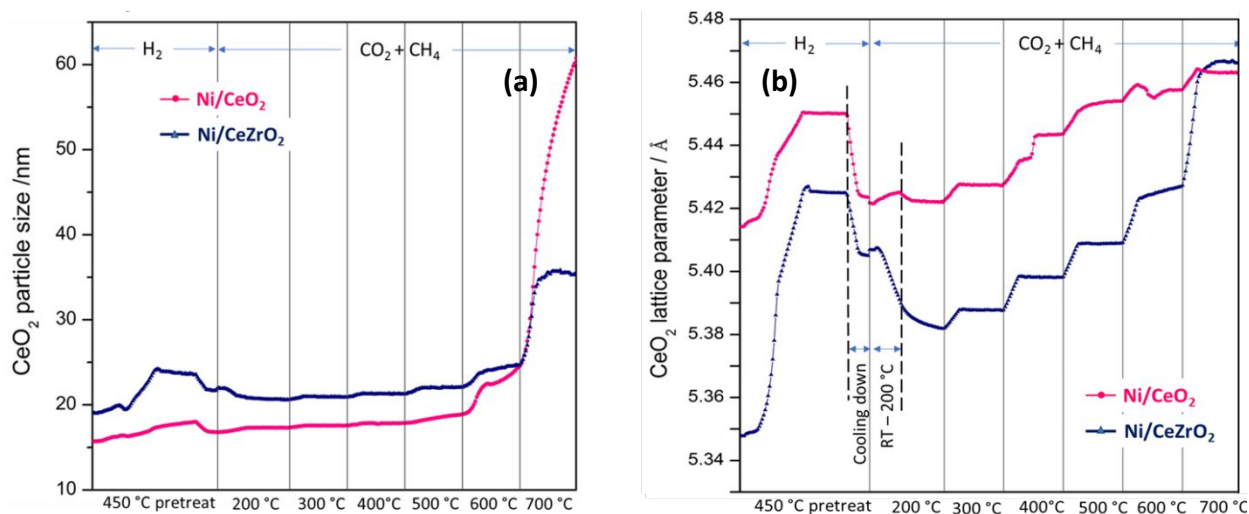


Figure 9. (a) Ceria particle size and (b) Ceria lattice parameter evolution during the methane dry reforming reaction. The results were generated from Rietveld refinement of the *in-situ* XRD data using the GSAS-II software.

The particle size of the active metallic Ni phase during the DRM reaction was also evaluated by Rietveld refinement and EXAFS fitting for Ni<sup>0</sup> particles in the Ni/CeO<sub>2</sub> and Ni/CeZrO<sub>2</sub> samples. The Fourier-transformed R-space EXAFS spectra of both Ni/CeZrO<sub>2</sub> and Ni/CeO<sub>2</sub>, are presented in Figure 7b and Figure S7, respectively and the fitting parameters are displayed in Table S2. The fitted coordination numbers of Ni atoms in the Ni/CeO<sub>2</sub> sample are 10.6 and 11.9 for the H<sub>2</sub> pretreated and under the DRM reaction at 700 °C, respectively, which are above the limit for the accurate estimation of the particle size using the half-sphere fcc packing model<sup>44</sup>. However, for the Ni/CeO<sub>2</sub>, the metallic Ni diffraction peaks (Figure 8b) are relatively larger and more intense than those in the Ni/CeZrO<sub>2</sub> (Figure 8a), thus enabling the Rietveld refinement to be performed on the Ni phase in Ni/CeO<sub>2</sub> to get an accurate Ni crystallite size. As for the Ni/CeZrO<sub>2</sub> sample, the smaller and broader diffraction peaks of the Ni phase make it difficult for accurate Rietveld refinement, thus EXAFS fittings were performed to obtain the coordination number of the Ni atoms and the results were further used to estimate the Ni particle size in the

Ni/CeZrO<sub>2</sub> catalyst, using the half-sphere fcc packing model.<sup>44</sup> Both the less pronounced Ni phase diffraction peaks and the small Ni atom coordination number in Ni/CeZrO<sub>2</sub> indicate smaller Ni particles than those in Ni/CeO<sub>2</sub>, which is verified by the summarized EXAFS fitting and Rietveld refinement results in Table 1. The metallic Ni particles in Ni/CeZrO<sub>2</sub> during the DRM reaction were estimated to be around 2.4 nm at room temperature and only increased to 3.5 nm at 700 °C. The Ni<sup>0</sup> particles in Ni/CeZrO<sub>2</sub> are smaller and exhibit a lower particle sintering extent at 700 °C under the DRM reaction, whereas the crystallite size of Ni/CeO<sub>2</sub> (calculated by Rietveld refinement) was 8 nm at room temperature and sintered to 11 nm at 700 °C. It should be pointed out that the estimation of the Ni particle size using the half-sphere fcc packing model<sup>44</sup> at 700 °C might result in a smaller Ni particle size due to the variation of the Debye–Waller factor at high temperatures than 25 °C. However, the estimated Ni particle size using either Rietveld refinement or the XAFS fitting agrees well with the particle size obtained from the TEM and EDS mapping images shown in Figure 2, suggesting that our methods for calculating the particle size are reliable. These results indicate that the presence of Zr in the ceria support improves the dispersion of Ni particles on the surface as well as diminishes Ni particle sintering at high temperature during the DRM reaction.

**Table 1.** Metallic Ni particle size in the Ni/CeZrO<sub>2</sub> and Ni/CeO<sub>2</sub> sample during the DRM reaction.

Ni <sup>0</sup> particle size (nm)	DRM at 25 °C	DRM at 700 °C
Ni/CeZrO <sub>2</sub>	2.4*	3.5*
Ni/CeO <sub>2</sub>	8#	11#

\* Calculated by EXAFS fitting; # Calculated by Rietveld refinement

Noticeably, a set of additional diffraction peaks at 4.0 ° and 6.5 ° appeared in the Ni/CeO<sub>2</sub> sample at 600 °C and intensified when the temperature increased to 700 °C (blue circled area in Figure 8b and the selected representative *in-situ* XRD patterns in Figure 10). This set of peaks could be assigned to a new ceria phase with an expanded lattice parameter (5.99 Å compared to 5.46 Å of the main ceria structure). As can be seen in Table 2, the peak at 4.0° with an interplanar spacing of 3.46 Å can be associated with the expanded (111) plane of the main structure ceria in the Ni/CeO<sub>2</sub> sample. The peak at 6.5° (d-spacing 2.12 Å) corresponds to the expanded (220) plane comparing to the main structure ceria peak at 7.2° (d-spacing 1.93 Å). The relationship between

1  
2  
3 the assigned (111) and (220) planes in the emerged new phase satisfied the structural relationship  
4 in the standard ceria face-cubic-centered structure, in which  $d_{111}/d_{220}$  equals to  $2\sqrt{2}/\sqrt{3}$ . This  
5 substantiates that our assignment of the emerged additional diffraction peaks to a lattice-expanded  
6 ceria phase is reasonable. The expansion of the ceria lattice in this new emerged phase could  
7 further be attributed to a migration of the surface Ni atoms into the ceria lattice, which partially  
8 replace the cerium sites. When a  $\text{Ce}^{4+}$  is substituted by a  $\text{Ni}^{2+}$ , an oxygen vacancy is created  
9 simultaneously to sustain the charge neutrality of the sample, and as previously discussed, the  
10 repulsion force between the oxygen vacancies and their surrounding cations consequently lead to  
11 the ceria lattice expansion.<sup>39, 45-46</sup> Thus, according to the above discussion, the set of additional  
12 diffraction peaks at  $4.0^\circ$  and  $6.5^\circ$  can be attributed to a partially doped nickel-ceria solid solution,  
13  $\text{Ce}_{1-x}\text{Ni}_x\text{O}_{2-y}$ . This type of mixed-oxide has been seen after heating mechanical mixtures of NiO-  
14  $\text{CeO}_2$ .<sup>47-49</sup> Diffraction peaks related to a  $\text{Ce}_{1-x}\text{Ni}_x\text{O}_{2-y}$  solid solution in Ni/CeZrO<sub>2</sub> (Figure 8a) are  
15 not as evident as in the Ni/CeO<sub>2</sub> sample. This implies that the introduction of Zr into the ceria  
16 support could inhibit or mitigate the diffusion of Ni into the ceria lattice and maintain the active  
17 metallic Ni phase on the surface.  
18  
19  
20  
21  
22  
23  
24  
25  
26  
27  
28  
29  
30  
31  
32  
33  
34  
35  
36  
37  
38  
39  
40  
41  
42  
43  
44  
45  
46  
47  
48  
49  
50  
51  
52  
53  
54  
55  
56  
57  
58  
59  
60

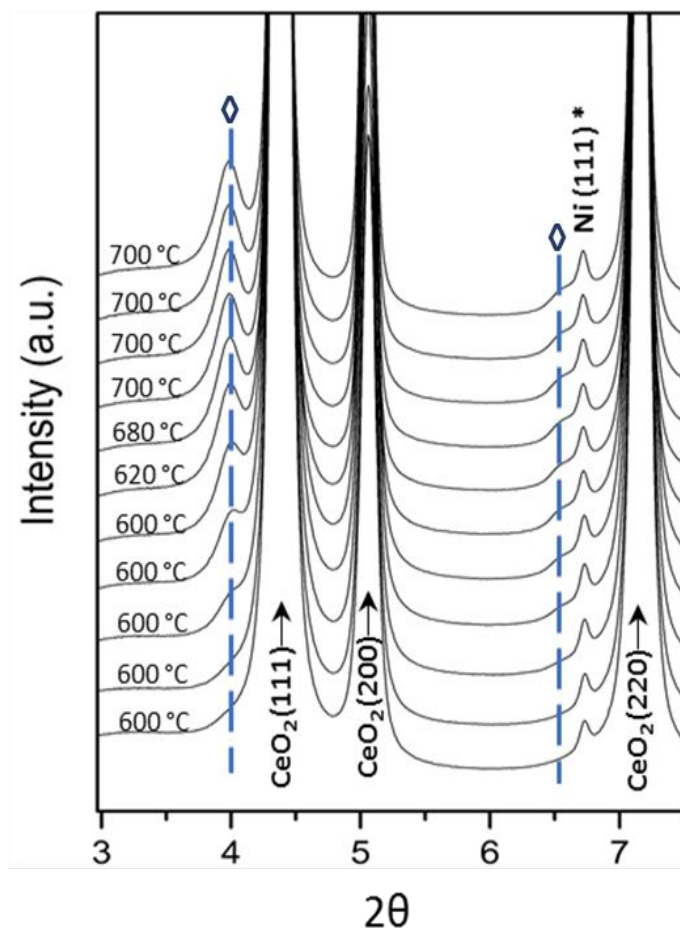


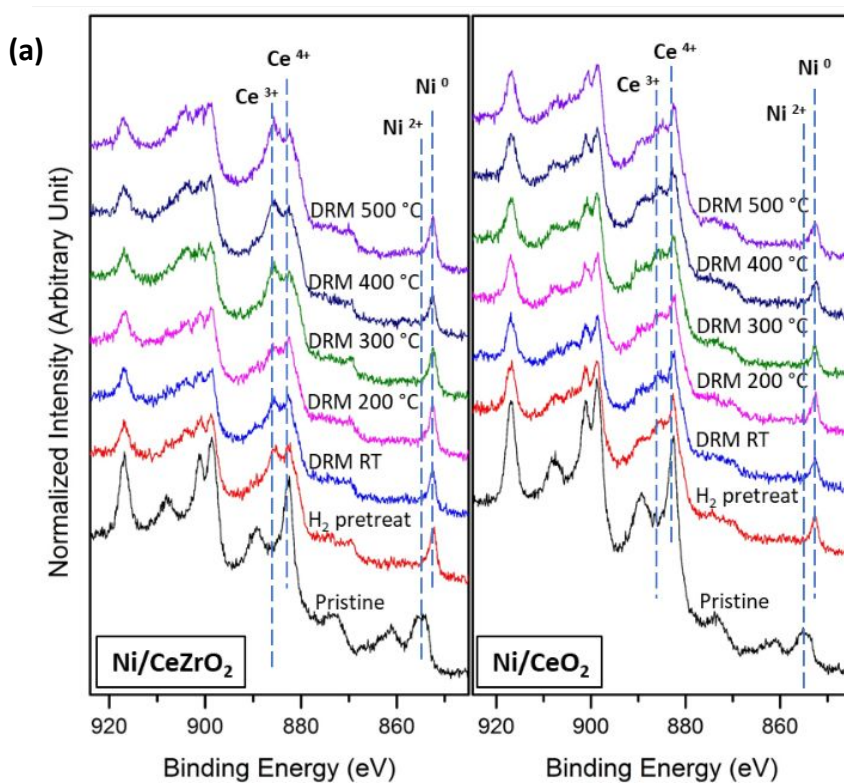
Figure 10. Selected *in-situ* XRD patterns of Ni/CeO<sub>2</sub> sample at and above 600 °C. The blue dashed lines mark out the emergence of a crystalline Ce<sub>1-x</sub>Ni<sub>x</sub>O<sub>2-y</sub> solid solution phase inside the Ni/CeO<sub>2</sub> sample during the DRM reaction at and above 600 °C.

**Table 2.** Interplanar spacing of main structure CeO<sub>2</sub> and the emerged new phase.

d-spacing (Å)	(111)	(220)	d <sub>111</sub> /d <sub>220</sub> (2√2/√3)
main CeO <sub>2</sub>	3.15	1.93	1.63
emerged phase (◊)	3.46	2.12	1.63

AP-XPS measurements were also performed on the Ni/CeZrO<sub>2</sub> and Ni/CeO<sub>2</sub> samples to monitor the dynamic changes of the sample surface under the DRM reaction conditions. The data for the Ce 3d and Ni 2p spectra of both samples are plotted in Figure 11a. As was observed in the *in-situ* XRD experiment, NiO was reduced to Ni<sup>0</sup> after H<sub>2</sub> reduction and the metallic Ni phase remained reduced during the DRM reaction at elevated temperatures for both Ni/CeO<sub>2</sub> and Ni/CeZrO<sub>2</sub>. The

less intense and broader Ni peaks in the Ni/CeO<sub>2</sub> sample suggests that less Ni sites (25% lower Ni peak area in Ni/CeO<sub>2</sub> than in Ni/CeZrO<sub>2</sub>) are exposed on the surface which was also observed in the Ni 2p AP-XPS spectra in a CH<sub>4</sub> atmosphere (Figure 6). Ce 3d spectra were fitted with Ce<sup>4+</sup> and Ce<sup>3+</sup> components (see Figure S8 and Table S3), and the concentration of Ce<sup>3+</sup> in both samples is plotted in Figure 11b. As can be seen from the plot, the ceria support was reduced after H<sub>2</sub> pretreatment for both samples, with a stronger Ce<sup>3+</sup> feature present in Ni/CeZrO<sub>2</sub> than in Ni/CeO<sub>2</sub>. The amount of Ce<sup>3+</sup> in Ni/CeO<sub>2</sub> near the sample surface remains at ~30%, which indicates that a dynamic equilibrium exists between the reduction and oxidation process exerted by CH<sub>4</sub> and CO<sub>2</sub> on the ceria surface, respectively. However, the surface Ce<sup>3+</sup> in Ni/CeZrO<sub>2</sub> sample was around 35% after H<sub>2</sub> reduction, and increased to ~43% when the temperature reached 300 °C, followed by a further slight increase to 45% at 500 °C. The higher fraction of Ce<sup>3+</sup> in Ni/CeZrO<sub>2</sub> sample during the DRM reaction reinforced the previous explanation that the introduction of Zr into the ceria support increases the reducibility of the support. Zr 3d spectra are also provided in Figure S7b, showing that Zr maintains a 4+ oxidation state throughout the whole DRM reaction and does not appear to be involved in the reaction through changes of its own oxidation state.



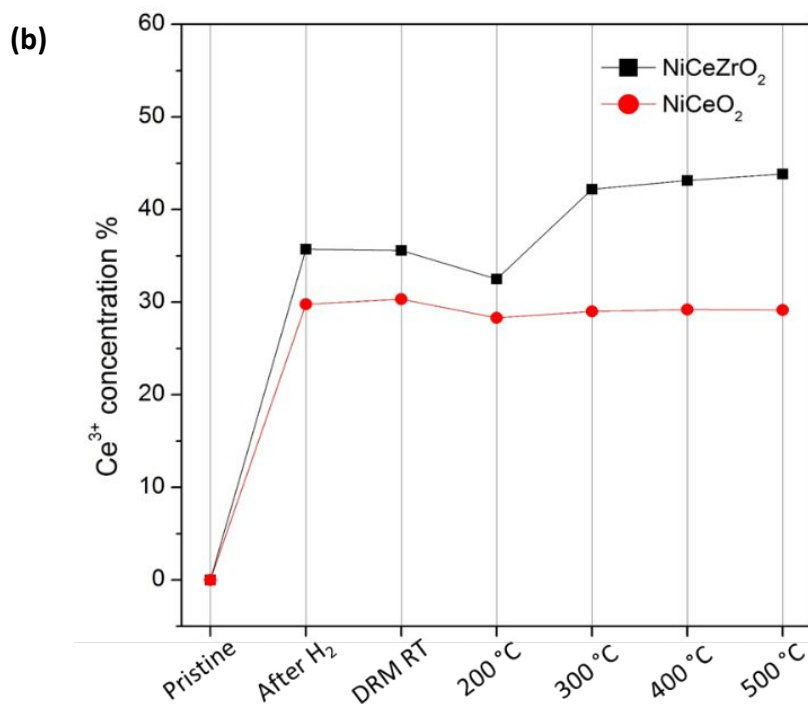


Figure 11. (a) Ce 3d and Ni 2p AP-XPS spectra of Ni/CeZrO<sub>2</sub> and Ni/CeO<sub>2</sub> samples under DRM reaction atmosphere at elevated temperatures. (b) Fraction of Ce<sup>3+</sup> in the catalysts at different temperatures under DRM conditions. Reaction conditions: 20 mTorr of H<sub>2</sub> were used to pretreat the samples at 450 °C for 30 min in the analysis chamber. After pumping down the H<sub>2</sub>, a 60 mTorr CH<sub>4</sub> + CO<sub>2</sub> 1:1 gas mixture was introduced into analysis chamber, and the spectra were collected at 25, 200, 300, 400 and 500 °C under this gas mixture. The Ce<sup>3+</sup> concentration was obtained through the AP-XPS spectra fitting and the error (% StDev) is below 5%, please refer to the supporting information for additional information.

The results presented above demonstrate that upon incorporation of Zr into the ceria support, the reducibility of this oxide was enhanced, which agrees with previously reported results.<sup>29, 50-51</sup> Furthermore, the improved reducibility facilitates CH<sub>4</sub> activation on the ceria surface as confirmed by the ceria lattice parameter changes during the *in-situ* XRD CH<sub>4</sub> activation measurement (Figure 5) and the AP-XPS results (Figure 6); It also results in a higher Ce<sup>3+</sup> content after H<sub>2</sub> pretreatment and under the DRM reaction conditions (Figure 11). In previous studies, the Ce<sup>3+</sup> was found to be the active site for CO<sub>2</sub> activation and oxidation of carbon species covering the surface of the catalyst during the DRM reaction.<sup>9-10, 52</sup> Thus, with more Ce<sup>3+</sup> present in ceria-

1  
2  
3 zirconia support, the CO<sub>2</sub> activation process was enabled, resulting in an elevated CO<sub>2</sub> conversion  
4 rate, and the carbon species on the Ni/CeZrO<sub>2</sub> sample surface was also decreased. The existence  
5 of Zr in the ceria support also helps to disperse metallic Ni particles (Figure 2 and Table 1) and  
6 maintains the structure of the ceria support. The latter is apparent by the relatively stable ceria  
7 particle size during the DRM reaction (Figure 9a) and the absence of Ni incorporation into the  
8 ceria support in the Ni/CeZrO<sub>2</sub> catalyst (Figure 8). The structurally stable ceria-zirconia support  
9 further helps to maintain a larger Ce<sup>3+</sup> content with more oxygen vacancies. Additionally it  
10 stabilizes the smaller metallic Ni particles, preserving their higher dispersion and adequate  
11 metallic nature on the sample surface.<sup>53-54</sup> Furthermore, throughout the DRM reaction, the small  
12 and stable Ni particles indicate a stronger metal-support interaction between Ni and the Zr doped  
13 ceria support. With the help of this strong interaction, metallic Ni particles appear rigidly  
14 anchored on the CeZrO<sub>2</sub> support, which inhibits particle sintering even at higher temperatures (up  
15 to 700 °C). Metallic Ni plays a pivotal role in the direct dissociation of CH<sub>4</sub>, and metal/support  
16 interfacial sites are claimed to be the active sites in CH<sub>4</sub> and CO<sub>2</sub> activation through redox  
17 reactions.<sup>21, 55</sup> Higher dispersion of metallic Ni particles on the sample surface provides more  
18 metallic Ni sites and metal/support interfacial sites available for interaction with CH<sub>4</sub> and CO<sub>2</sub>  
19 reactant gases. These sites, combined with the metal-support interaction, which promotes the  
20 electron and oxygen mobility in the catalyst, lead to an improved turnover of CH<sub>4</sub> and CO<sub>2</sub> and  
21 higher production rate of CO + H<sub>2</sub>.<sup>10, 52, 56-57</sup>

## 32 CONCLUSION

33  
34  
35  
36  
37  
38  
39 In this work the effects of Zr-doping of the ceria support for the methane dry reforming reaction  
40 was comprehensively investigated on Ni/CeO<sub>2</sub> and Ni/CeZrO<sub>2</sub> catalysts. By introducing Zr as the  
41 dopant, the catalytic performance including conversion, reaction rate, and H<sub>2</sub> selectivity were  
42 significantly enhanced. The *in-situ* characterizations of the catalysts during difficult DRM  
43 reaction conditions depict the dynamic chemical and structural changes Ni and Ce go through,  
44 with and without the Zr dopant. The results reveal details about the mechanism for the enhanced  
45 DRM catalytic performance achieved with Zr doping. By doping Zr into the ceria support, a larger  
46 Ce<sup>3+</sup> content was observed in the mixed-oxide support upon reaction with pure CH<sub>4</sub> or during  
47 DRM, indicating a higher reducibility of the mixed-oxide support. The particle sintering process  
48 of both Ni and ceria was effectively hindered. A stable ceria structure with the Zr dopant was  
49  
50  
51  
52  
53  
54  
55  
56  
57  
58  
59  
60

1  
2  
3 preserved without any active metallic Ni incorporation into the support. The smaller nickel  
4 particles expose a larger amount of active metallic Ni surface and Ni-CeO<sub>2</sub> interfacial sites for  
5 CH<sub>4</sub> and CO<sub>2</sub> activation. The small and well-dispersed metallic Ni particles interact strongly with  
6 the highly reduced, yet structurally stable, ceria-zirconia support in the Ni/CeZrO<sub>2</sub> catalysts. All  
7 of this coalesces to result in an enhanced reaction activity and H<sub>2</sub> selectivity for the dry reforming  
8 of methane reaction.  
9  
10  
11  
12  
13  
14

## 15 ASSOCIATED CONTENT

16  
17 Calculations of the conversions, reaction rates and selectivity; PDF spectra of Ni/CeZrO<sub>2</sub> and  
18 Ni/CeO<sub>2</sub> samples with ZrO<sub>2</sub>, CeO<sub>2</sub> PDF profiles as references; TEM images of the Ni/CeO<sub>2</sub>  
19 sample after the DRM reaction at 700 °C for 1h; Residual gas analyzer spectra of the Ni/CeZrO<sub>2</sub>  
20 and Ni/CeO<sub>2</sub> under the DRM reaction; Temperature programmed reduction (H<sub>2</sub>-TPR) of Ni/CeO<sub>2</sub>  
21 and 4 Ni/CeZrO<sub>2</sub> catalysts; Fitted Ni 2p AP-XPS spectra of Ni/CeZrO<sub>2</sub> and Ni/CeO<sub>2</sub> samples  
22 under CH<sub>4</sub> atmosphere with elevated temperatures and the fitting results; AP-XPS results of Zr  
23 3d spectra during CH<sub>4</sub>-temperature programmed reduction and DRM reaction process; The  
24 Fourier-transformed R-space EXAFS spectra and Ni K-edge EXAFS fitting results of Ni/CeO<sub>2</sub>  
25 and Ni/CeZrO<sub>2</sub> samples after H<sub>2</sub> pretreatment and under DRM reaction at 700 °C; Fitted Ce 3d  
26 AP-XPS spectra of Ni/CeZrO<sub>2</sub> and Ni/CeO<sub>2</sub> samples under DRM reaction condition and the  
27 fitting results and details.  
28  
29  
30  
31  
32  
33  
34  
35  
36  
37

## 38 ACKNOWLEDGEMENTS

39  
40 The work carried out at Brookhaven National Laboratory was supported by the US Department  
41 of Energy under contract no. DE-SC0012704. S.D.S. is supported by a US Department of Energy  
42 Early Career Award. The PDF measurement used resources 28ID-1 of the National Synchrotron  
43 Light Source II, a U.S. Department of Energy (DOE) Office of Science User Facility operated for  
44 the DOE Office of Science by Brookhaven National Laboratory under Contract No. DE-  
45 SC0012704. This research also used resources of the Center for Functional Nanomaterials,  
46 specifically the electron microscopy facilities which is a U.S. DOE Office of Science Facility, at  
47 Brookhaven National Laboratory under Contract No. DE-SC0012704. The XRD and XAFS  
48 experiments used resources of the Advanced Photon Source Beamline 17BM (XRD) and 20ID  
49 (XAFS) at Argonne National Laboratory, which is an Office of Science User Facility operated  
50  
51  
52  
53  
54  
55  
56  
57

for the U.S. Department of Energy (DOE) Office of Science and was supported by the U.S. DOE under Contract No. DE-AC02-06CH11357, and the Canadian Light Source and its funding partners. Janvit Teržan, Kristijan Lorber, and Petar Djinović are funded by Slovenian national research agency (ARRS) through research program P2-150 and projects J2-1726 and BI-US/18-20-004.

## REFERENCES

1. Aramouni, N. A. K.; Touma, J. G.; Tarboush, B. A.; Zeaiter, J.; Ahmad, M. N. *Catalyst design for dry reforming of methane: Analysis review. Renew. Sust. Energ. Rev.* **2018**, *82*, 2570-2585.
2. Jang, W.-J.; Shim, J.-O.; Kim, H.-M.; Yoo, S.-Y.; Roh, H.-S. *A review on dry reforming of methane in aspect of catalytic properties. Catal. Today* **2019**, *324*, 15-26.
3. Ross, J. R. H. *Contemporary Catalysis*, Ross, J. R. H., Ed. Elsevier: Amsterdam, 2019, 251-272.
4. Pachauri, R. K.; Allen, M. R.; Barros, V. R.; Broome, J.; Cramer, W.; Christ, R.; Church, J. A.; Clarke, L.; Dahe, Q.; Dasgupta, P. *Climate change 2014: synthesis report. Contribution of Working Groups I, II and III to the fifth assessment report of the Intergovernmental Panel on Climate Change*. Ipcc: 2014.
5. Fan, M. S.; Abdullah, A. Z.; Bhatia, S. *Catalytic technology for carbon dioxide reforming of methane to synthesis gas. ChemCatChem* **2009**, *1*, 192-208.
6. Cavenati, S.; Grande, C. A.; Rodrigues, A. E. *Separation of CH<sub>4</sub>/CO<sub>2</sub>/N<sub>2</sub> mixtures by layered pressure swing adsorption for upgrade of natural gas. Chem. Eng. Sci.* **2006**, *61*, 3893-3906.
7. Zhang, F.; Liu, Z.; Zhang, S.; Akter, N.; Palomino, R. M.; Vovchok, D.; Orozco, I.; Salazar, D.; Rodriguez, J. A.; Llorca, J. *In Situ Elucidation of the Active State of Co–CeO<sub>x</sub> Catalysts in the Dry Reforming of Methane: The Important Role of the Reducible Oxide Support and Interactions with Cobalt. ACS.Catal.* **2018**, *8*, 3550-3560.
8. Zhang, F.; Yao, S.; Liu, Z.; Gutiérrez, R. A.; Vovchok, D.; Cen, J.; Xu, W.; Ramírez, P. J.; Kim, T.; Senanayake, S. D.; Rodriguez, J. A. *Reaction of Methane with MO<sub>x</sub>/CeO<sub>2</sub> (M = Fe, Ni, and Cu) Catalysts: In Situ Studies with Time-Resolved X-ray Diffraction. J. Phys. Chem. C* **2018**, *122*, 28739-28747.
9. Liu, Z.; Grinter, D. C.; Lustemberg, P. G.; Nguyen-Phan, T.-D.; Zhou, Y.; Luo, S.; Waluyo, I.; Crumlin, E. J.; Stacchiola, D. J.; Zhou, J.; Carrasco, J.; Busnengo, H. F.; Ganduglia-Pirovano, M. V.; Senanayake, S. D.; Rodriguez, J. A. *Dry Reforming of Methane on a Highly-Active Ni-CeO<sub>2</sub> Catalyst: Effects of Metal-Support Interactions on C–H Bond Breaking. Angew. Chem. Int. Ed.* **2016**, *128*, 7581-7585.
10. Liu, Z.; Zhang, F.; Rui, N.; Li, X.; Lin, L.; Betancourt, L. E.; Su, D.; Xu, W.; Cen, J.; Attenkofer, K.; Idriss, H.; Rodriguez, J. A.; Senanayake, S. D. *Highly Active Ceria-Supported Ru Catalyst for the Dry Reforming of Methane: In Situ Identification of Ru $\delta^+$ –Ce<sup>3+</sup> Interactions for Enhanced Conversion. ACS.Catal.* **2019**, *9*, 3349-3359.
11. Farmer, J. A.; Campbell, C. T. *Ceria Maintains Smaller Metal Catalyst Particles by Strong Metal-Support Bonding. Science* **2010**, *329*, 933-936.
12. Basile, F.; Mafessanti, R.; Fasolini, A.; Fornasari, G.; Lombardi, E.; Vaccari, A. *Effect of synthetic method on CeZr support and catalytic activity of related Rh catalyst in the oxidative reforming reaction. J. Eur. Ceram. Soc.* **2019**, *39*, 41-52.
13. Djinović, P.; Črnivec, I. G. O.; Pintar, A. *Biogas to syngas conversion without carbonaceous deposits via the dry reforming reaction using transition metal catalysts. Catal. Today* **2015**, *253*, 155-162.
14. Wang, Y.; Liang, S.; Cao, A.; Thompson, R. L.; Veser, G. *Au-mixed lanthanum/cerium oxide catalysts for water gas shift. Appl. Catal., B* **2010**, *99*, 89-95.

15. Liu, Z.; Xu, W.; Yao, S.; C. Johnson-Peck, A.; Zhao, F.; Michorczyk, P.; Kubacka, A.; Stach, E.; Fernández-García, M.; Senanayake, S.; A. Rodriguez, J. *Superior performance of Ni–W–Ce mixed-metal oxide catalysts for ethanol steam reforming: Synergistic effects of W- and Ni-dopants*. *J. Catal.* **2015**, 321, 90-99.
16. Razzaq, R.; Zhu, H.; Jiang, L.; Muhammad, U.; Li, C.; Zhang, S. *Catalytic methanation of CO and CO<sub>2</sub> in coke oven gas over Ni–Co/ZrO<sub>2</sub>–CeO<sub>2</sub>*. *Ind. Eng. Chem. Res.* **2013**, 52, 2247-2256.
17. Le, M. C.; Van, K. L.; Nguyen, T. H. T.; Nguyen, N. H. *The Impact of Ce-Zr Addition on Nickel Dispersion and Catalytic Behavior for CO<sub>2</sub> Methanation of Ni/AC Catalyst at Low Temperature*. *J. Chem.* **2017**, 2017, 11.
18. Kambolis, A.; Matralis, H.; Trovarelli, A.; Papadopoulou, C. *Ni/CeO<sub>2</sub>-ZrO<sub>2</sub> catalysts for the dry reforming of methane*. *Appl. Catal., A* **2010**, 377, 16-26.
19. Wang, F.; Xu, L.; Yang, J.; Zhang, J.; Zhang, L.; Li, H.; Zhao, Y.; Li, H. X.; Wu, K.; Xu, G. Q.; Chen, W. *Enhanced catalytic performance of Ir catalysts supported on ceria-based solid solutions for methane dry reforming reaction*. *Catal. Today* **2017**, 281, 295-303.
20. Mullen, G. M.; Evans, E. J.; Siegert, B. C.; Miller, N. R.; Rosselet, B. K.; Sabzevari, I.; Brush, A.; Duan, Z.; Buddie Mullins, C. *The interplay between ceria particle size, reducibility, and ethanol oxidation activity of ceria-supported gold catalysts*. *React. Chem. Eng.* **2018**, 3, 75-85.
21. Boaro, M.; Colussi, S.; Trovarelli, A. *Ceria-Based Materials in Hydrogenation and Reforming Reactions for CO(2) Valorization*. *Front. Chem.* **2019**, 7, 28-28.
22. Farrow, C.; Juhas, P.; Liu, J.; Bryndin, D.; Božin, E.; Bloch, J.; Proffen, T.; Billinge, S. *PDFfit2 and PDFgui: computer programs for studying nanostructure in crystals*. *J. Phys.: Condens. Matter* **2007**, 19, 335219.
23. Chupas, P. J.; Chapman, K. W.; Kurtz, C.; Hanson, J. C.; Lee, P. L.; Grey, C. P. *A versatile sample-environment cell for non-ambient X-ray scattering experiments*. *J. Appl. Crystallogr.* **2008**, 41, 822-824.
24. Toby, B. H.; Von Dreele, R. B. *GSAS-II: the genesis of a modern open-source all purpose crystallography software package*. *J. Appl. Crystallogr.* **2013**, 46, 544-549.
25. Ravel, B.; Newville, M. *ATHENA, ARTEMIS, HEPHAESTUS: data analysis for X-ray absorption spectroscopy using IFEFFIT*. *J. Synchrotron Radiat.* **2005**, 12, 537-541.
26. Palomino, R. M.; Hamlyn, R.; Liu, Z.; Grinter, D. C.; Waluyo, I.; Rodriguez, J. A.; Senanayake, S. D. *Interfaces in heterogeneous catalytic reactions: Ambient pressure XPS as a tool to unravel surface chemistry*. *J. Electron Spectrosc. Relat. Phenom.* **2017**, 221, 28-43.
27. Sadykov, V. A.; Simonov, M. N.; Mezentseva, N. V.; Pavlova, S. N.; Fedorova, Y. E.; Bobin, A. S.; Bepalko, Y. N.; Ishchenko, A. V.; Krieger, T. A.; Glazneva, T. S.; V., L. T.; Cherepanova, S. V.; Kaichev, V. V.; Saraev, A. A.; Chesalov, Y. A.; Shmakov, A. N.; Roger, A.-C.; Adamski, A. *Ni-loaded nanocrystalline ceria-zirconia solid solutions prepared via modified Pechini route as stable to coking catalysts of CH<sub>4</sub> dry reforming*. *Open Chem.* **2016**, 14, 363.
28. Priya, N. S.; Somayaji, C.; Kanagaraj, S. *Optimization of Ceria-Zirconia Solid Solution based on OSC Measurement by Cyclic Heating Process*. *Procedia Eng.* **2013**, 64, 1235-1241.
29. Djinović, P.; Črnivec, I. G. O.; Erjavec, B.; Pintar, A. *Details Behind the Self-Regeneration of Supported NiCo/Ce<sub>0.8</sub>Zr<sub>0.2</sub>O<sub>2</sub> Bimetallic Catalyst in the CH<sub>4</sub>–CO<sub>2</sub> Reforming Reaction*. *ChemCatChem* **2014**, 6, 1652-1663.
30. Li, H.; Zhu, Q.; Li, Y.; Gong, M.; Chen, Y.; Wang, J.; Chen, Y. *Effects of ceria/zirconia ratio on properties of mixed CeO<sub>2</sub>-ZrO<sub>2</sub>-Al<sub>2</sub>O<sub>3</sub> compound*. *J. Rare Earths* **2010**, 28, 79-83.
31. Gateshki, M.; Niederberger, M.; Deshpande, A. S.; Ren, Y.; Petkov, V. *Atomic-scale structure of nanocrystalline CeO<sub>2</sub>-ZrO<sub>2</sub> oxides by total x-ray diffraction and pair distribution function analysis*. *J. Phys.: Condens. Matter* **2007**, 19, 156205.
32. Pakhare, D.; Spivey, J. *A review of dry (CO<sub>2</sub>) reforming of methane over noble metal catalysts*. *Chem. Soc. Rev.* **2014**, 43, 7813-7837.

- 1  
2  
3 33. Caravella, A.; Brunetti, A.; Grandinetti, M.; Barbieri, G. *Dry Reforming of Methane in a Pd-Ag Membrane Reactor: Thermodynamic and Experimental Analysis*. *ChemEngineering* **2018**, *2*, 48.
- 4 34. Khairudin, N. F.; Sukri, M. F. F.; Khavarian, M.; Mohamed, A. R. *Understanding the performance and mechanism of Mg-containing oxides as support catalysts in the thermal dry reforming of methane*. *Beilstein J. Nanotechnol.* **2018**, *9*, 1162-1183.
- 5 35. Pakhare, D.; Spivey, J. *A review of dry (CO<sub>2</sub>) reforming of methane over noble metal catalysts*. *Chem. Soc. Rev.* **2014**, *43*, 7813-7837.
- 6 36. Arora, S.; Prasad, R. *An overview on dry reforming of methane: strategies to reduce carbonaceous deactivation of catalysts*. *RSC Adv.* **2016**, *6*, 108668-108688.
- 7 37. Usman, M.; Wan Daud, W. M. A.; Abbas, H. F. *Dry reforming of methane: Influence of process parameters—A review*. *Renew. Sust. Energ. Rev.* **2015**, *45*, 710-744.
- 8 38. Mogensen, M.; Sammes, N. M.; Tompsett, G. A. *Physical, chemical and electrochemical properties of pure and doped ceria*. *Solid State Ionics* **2000**, *129*, 63-94.
- 9 39. Marrocchelli, D.; Bishop, S. R.; Tuller, H. L.; Yildiz, B. *Understanding Chemical Expansion in Non - Stoichiometric Oxides: Ceria and Zirconia Case Studies*. *Adv. Funct. Mater.* **2012**, *22*, 1958-1965.
- 10 40. Barsoum, M.; Barsoum, M. *Fundamentals of ceramics*. CRC press: 2002.
- 11 41. Rafique, A.; Raza, R.; Arifin, N. A.; Ullah, M. K.; Ali, A.; Steinberger-Wilckens, R. *Electrochemical and thermal characterization of doped ceria electrolyte with lanthanum and zirconium*. *Ceram. Int.* **2018**, *44*, 6493-6499.
- 12 42. Laachir, A.; Perrichon, V.; Badri, A.; Lamotte, J.; Catherine, E.; Lavalley, J. C.; El Fallah, J.; Hilaire, L.; Le Normand, F.; Quéméré, E.; Sauvion, G. N.; Touret, O. *Reduction of CeO<sub>2</sub> by hydrogen. Magnetic susceptibility and Fourier-transform infrared, ultraviolet and X-ray photoelectron spectroscopy measurements*. *J. Chem. Soc., Faraday Trans.* **1991**, *87*, 1601-1609.
- 13 43. López, J. M.; Gilbank, A. L.; García, T.; Solsona, B.; Agouram, S.; Torrente-Murciano, L. *The prevalence of surface oxygen vacancies over the mobility of bulk oxygen in nanostructured ceria for the total toluene oxidation*. *Appl. Catal., B* **2015**, *174*, 403-412.
- 14 44. Beale, A. M.; Weckhuysen, B. M. *EXAFS as a tool to interrogate the size and shape of mono and bimetallic catalyst nanoparticles*. *PCCP* **2010**, *12*, 5562-5574.
- 15 45. Hong, S. J.; Virkar, A. V. *Lattice Parameters and Densities of Rare-Earth Oxide Doped Ceria Electrolytes*. *J. Am. Ceram. Soc.* **1995**, *78*, 433-439.
- 16 46. Derafa, W.; Paloukis, F.; Mewafy, B.; Baaziz, W.; Ersen, O.; Petit, C.; Corbel, G.; Zafeiratos, S. *Synthesis and characterization of nickel-doped ceria nanoparticles with improved surface reducibility*. *RSC Adv.* **2018**, *8*, 40712-40719.
- 17 47. Zhou, Y.; Zhou, J. *Interactions of Ni Nanoparticles with Reducible CeO<sub>2</sub>(111) Thin Films*. *J. Phys. Chem. C* **2012**, *116*, 9544-9549.
- 18 48. Senanayake, S. D.; Evans, J.; Agnoli, S.; Barrio, L.; Chen, T.-L.; Hrbek, J.; Rodriguez, J. A. *Water-Gas Shift and CO Methanation Reactions over Ni-CeO<sub>2</sub>(111) Catalysts*. *Top. Catal.* **2011**, *54*, 34-41.
- 19 49. Barrio, L.; Kubacka, A.; Zhou, G.; Estrella, M.; Martínez-Arias, A.; Hanson, J. C.; Fernández-García, M.; Rodriguez, J. A. *Unusual Physical and Chemical Properties of Ni in Ce<sub>1-x</sub>Ni<sub>x</sub>O<sub>2-y</sub> Oxides: Structural Characterization and Catalytic Activity for the Water Gas Shift Reaction*. *J. Phys. Chem. C* **2010**, *114*, 12689-12697.
- 20 50. Wang, R.; Fang, M. *Improved low-temperature reducibility in ceria zirconia nanoparticles by redox treatment*. *J. Mater. Chem.* **2012**, *22*, 1770-1773.
- 21 51. Aribi, K.; Soltani, Z.; Ghelamallah, M.; Granger, P. *Structure, morphology and reducibility of ceria-doped zirconia*. *J. Mol. Struct.* **2018**, *1156*, 369-376.
- 22 52. Zhang, F.; Liu, Z.; Zhang, S.; Akter, N.; Palomino, R. M.; Vovchok, D.; Orozco, I.; Salazar, D.; Rodriguez, J. A.; Llorca, J.; Lee, J.; Kim, D.; Xu, W.; Frenkel, A. I.; Li, Y.; Kim, T.; Senanayake, S. D. *In Situ*
- 23  
24  
25  
26  
27  
28  
29  
30  
31  
32  
33  
34  
35  
36  
37  
38  
39  
40  
41  
42  
43  
44  
45  
46  
47  
48  
49  
50  
51  
52  
53  
54  
55  
56  
57  
58  
59  
60

1  
2  
3 *Elucidation of the Active State of Co–CeO<sub>x</sub> Catalysts in the Dry Reforming of Methane: The Important Role*  
4 *of the Reducible Oxide Support and Interactions with Cobalt. ACS.Catal. 2018, 8, 3550-3560.*

5 53. Zhou, X.-D.; Huebner, W. *Size-induced lattice relaxation in CeO<sub>2</sub> nanoparticles. Appl. Phys. Lett.*  
6 **2001**, 79, 3512-3514.

7  
8 54. Deshpande, S.; Patil, S.; Kuchibhatla, S. V.; Seal, S. *Size dependency variation in lattice parameter*  
9 *and valency states in nanocrystalline cerium oxide. Appl. Phys. Lett. 2005, 87, 133113.*

10 55. Rodriguez, J. A.; Grinter, D. C.; Liu, Z.; Palomino, R. M.; Senanayake, S. D. *Ceria-based model*  
11 *catalysts: fundamental studies on the importance of the metal–ceria interface in CO oxidation, the water–*  
12 *gas shift, CO<sub>2</sub> hydrogenation, and methane and alcohol reforming. Chem. Soc. Rev. 2017, 46, 1824-1841.*

13 56. Smirnova, M. Y.; Bobin, A. S.; Pavlova, S. N.; Ishchenko, A. V.; Selivanova, A. V.; Kaichev, V. V.;  
14 Cherepanova, S. V.; Krieger, T. A.; Arapova, M. V.; Roger, A.-C.; Adamski, A.; Sadykov, V. A. *Methane dry*  
15 *reforming over Ni catalysts supported on Ce–Zr oxides prepared by a route involving supercritical fluids.*  
16 *Open Chem. 2017, 15, 412.*

17  
18 57. Simonov, M. N.; Rogov, V. A.; Smirnova, M. Y.; Sadykov, V. A. *Pulse Microcalorimetry Study of*  
19 *Methane Dry Reforming Reaction on Ni/Ceria-Zirconia Catalyst. Catalysts 2017, 7, 268.*

## TOC

